



**Ground-based
middle-atmospheric
wind radiometry**

R. Rüfenacht et al.

This discussion paper is/has been under review for the journal Atmospheric Measurement Techniques (AMT). Please refer to the corresponding final paper in AMT if available.

Middle-atmospheric zonal and meridional wind profiles from polar, tropical and mid latitudes with the ground-based microwave Doppler wind radiometer WIRA

R. Rüfenacht¹, A. Murk¹, N. Kämpfer¹, P. Eriksson², and S. A. Buehler^{3,*}

¹Institute of Applied Physics, University of Bern, Bern, Switzerland

²Department of Earth and Space Sciences, Chalmers University of Technology, Gothenburg, Sweden

³Division of Space Technology, SRT, Luleå University of Technology, Kiruna, Sweden

* now at: Meteorological Institute, Center for Earth System Research and Sustainability, University of Hamburg, Hamburg, Germany

Received: 4 July 2014 – Accepted: 11 July 2014 – Published: 28 July 2014

Correspondence to: R. Rüfenacht (rolf.ruefenacht@iap.unibe.ch)

Published by Copernicus Publications on behalf of the European Geosciences Union.

Title Page

Abstract

Introduction

Conclusions

References

Tables

Figures



Back

Close

Full Screen / Esc

Printer-friendly Version

Interactive Discussion



Abstract

WIRA is a ground-based microwave Doppler spectro radiometer specifically designed for the measurement of profiles of horizontal wind in the upper stratosphere and lower mesosphere region where no other continuously running measurement technique exists. A proof of principle has been delivered in a previous publication. Since a technical upgrade which improved the signal to noise ratio by a factor of 2.4 the full horizontal wind field comprising zonal and meridional wind profiles is continuously measured. A completely new retrieval based on optimal estimation has been set up. Its characteristics are detailed in the present paper.

Since the start of the routine operation of the first prototype in September 2010, WIRA has been measuring at four different locations at polar, mid and tropical latitudes for time periods between 5.5 and 11 months. A comparison between the data series from WIRA and ECMWF model data revealed agreement within 10 % in the stratospheric zonal wind. The meridional wind profiles agree within their error bars over the entire sensitive altitude range of WIRA. However, significant differences in the mesospheric zonal wind speed of up to 40 % have been found.

1 Introduction

Wind is a key parameter for the characterisation of the atmosphere and its dynamics on every altitude level. Recent studies have also demonstrated the influence of middle-atmospheric dynamics on tropospheric weather patterns (e.g. Baldwin and Dunkerton, 2001; Hardiman et al., 2011). However, in the middle atmosphere the only continuous source of wind data so far were models. A gap region with a lack of measured wind information exists in the the middle atmosphere between approximately 10 and 10^{-2} hPa. Only very few measurement techniques covering parts of this altitude range are or have been operated on campaign basis. Measurements from Rayleigh lidars (Baumgarten, 2010), rocket aided techniques (Goldberg et al., 2004; Chu et al., 2007)

AMTD

7, 7717–7752, 2014

Ground-based middle-atmospheric wind radiometry

R. Rüfenacht et al.

Title Page

Abstract

Introduction

Conclusions

References

Tables

Figures



Back

Close

Full Screen / Esc

Printer-friendly Version

Interactive Discussion



and a 230 GHz astronomical telescope (Burrows, 2007) have been reported. A more extended overview of the different wind measurement techniques with their key characteristics and their sensitive altitude range can be found in Rufenacht et al. (2012).

A first prototype of the wind radiometer WIRA has demonstrated the potential of the ground-based microwave Doppler wind radiometry (Rufenacht et al., 2012). Compared to the other techniques mentioned above, ground-based microwave radiometry has the advantage to allow the acquisition of long continuous time series of wind profiles. Indeed, the operation of such instruments can be highly automated and remotely controlled. Moreover, microwave radiometry is not dependent on daylight conditions and only weakly affected by cloud cover.

Since the first prototype of WIRA described in Rufenacht et al. (2012) significant technical developments as well as a completely new retrieval algorithm have greatly enhanced the quality of the wind estimates. Together with the data obtained on extended measurement campaigns held at polar, tropical and mid latitudes, this gives us the ability to draw meaningful conclusions on the difference between measured middle-atmospheric wind and data from models.

The first part of the present publication will describe the key characteristics of the receiver focussing on the new technical developments, while the second part introduces the new optimal estimation retrieval. In the third part wind data from the different measurement campaigns are presented and compared to model data from ECMWF.

2 The instrument

The ground-based wind radiometer WIRA (see Fig. 1) is a 142 GHz heterodyne radiometer measuring Doppler shifts in the emission spectrum of atmospheric ozone in order to derive middle-atmospheric wind profiles. In the routine operation the duration of one measurement cycle is 60 s. Such a cycle contains the measurement of the signals from the two calibration targets (ambient temperature load and sky at zenith) as well as from two or four cardinal directions for the wind retrieval. The wind retrieval

Ground-based middle-atmospheric wind radiometry

R. Rufenacht et al.

Title Page

Abstract

Introduction

Conclusions

References

Tables

Figures



Back

Close

Full Screen / Esc

Printer-friendly Version

Interactive Discussion



combines the calibrated spectra obtained at two opposite viewing directions (i.e. east and west for zonal and north and south for meridional wind). In this way drifts and fluctuations in reference frequency oscillators on timescales larger than one minute are removed in the wind retrieval.

The prototype of the instrument as well as its operation mode and calibration scheme is described in detail in Rüfenacht et al. (2012). A block diagram of the current version of WIRA is shown in Fig. 2. Since the first prototype different frequency sources have been replaced mainly for the sake of operational robustness. This also led to minor improvements in the total frequency stability. A re-assessment of the frequency stability has been performed after the last upgrade by using a GPS signal as frequency reference. With this setup Allan standard deviation measurements revealed the results displayed in Fig. 3. As drifts and longterm frequency instabilities on timescales longer than one measurement cycle are compensated by the comparison of spectra from opposite viewing directions in the wind retrieval, we can state that the maximum frequency error induced by reference oscillator instabilities is smaller than 14 Hz. This leads to a wind error of a few centimeters per second only and can thus safely be neglected in the error analysis.

For reasons of compactness and reliability, especially when measuring under harsh conditions, WIRA cannot use an optical sideband filter. Therefore, the instrument was initially designed as a double sideband radiometer. Benefitting from recent advances in the construction of low noise amplifiers (LNA) at frequencies beyond 100 GHz WIRA was transformed to a single sideband radiometer in summer 2012 by adding a D-band LNA, a waveguide bandpass filter and an isolator before the radio frequency (RF) entrance of the mixer. S-parameter measurements using a high frequency vector network analyser revealed a good sideband separation achieved by the new RF components. The image sideband centered around 149.576 GHz is rejected down to 50 dB and the reflections in the signal sideband are in the order of -30 dB only.

Noise temperature tests with liquid nitrogen calibrations revealed that the upgrade had reduced the noise temperature from 880 K double sideband to 740 K single

**Ground-based
middle-atmospheric
wind radiometry**

R. Rüfenacht et al.

Title Page

Abstract

Introduction

Conclusions

References

Tables

Figures



Back

Close

Full Screen / Esc

Printer-friendly Version

Interactive Discussion



sideband. As the contribution of the image sideband in a double sideband receiver can be regarded as noise, the change in the receiver noise temperature corresponds to a 2.4 times better signal to noise ratio for the upgraded instrument.

The optics of WIRA had been designed for the measurement of the complete horizontal wind field, i.e. for the measurement of the zonal and meridional wind component. However, because of the relatively low signal to noise ratio, the meridional wind which is generally small had not been routinely measured until summer 2012 in order to save integration time in order to get a more accurate estimate of the zonal wind. After the instrumental upgrade WIRA routinely measures both the zonal and the meridional wind component.

3 Optimal estimation wind retrieval

A first approach for a wind retrieval from spectra measured by a ground-based microwave radiometer was presented in Rüfenacht et al. (2012). This somewhat simplistic approach which assumed five completely independent atmospheric levels has now been replaced by a retrieval algorithm based on full radiative transfer modeling of the atmosphere coupled with the optimal estimation method for inverse problems (Rodgers, 2000).

The signal observed by a ground based microwave radiometer is a superposition of emissions and absorptions at different atmospheric altitudes along the line of sight path s . The measured brightness temperature T_b measured at the frequency ν can be described by

$$T_b(\nu) = T_{b0}(\nu)e^{-\tau(s_0)} + \int_0^{s_0} k_a(\nu, \rho(s), T(s), n_i(s), \Delta\nu(s), \dots) \cdot T(s)e^{-\tau(s)} \cdot ds \quad (1)$$

Ground-based middle-atmospheric wind radiometry

R. Rüfenacht et al.

Title Page

Abstract

Introduction

Conclusions

References

Tables

Figures

◀

▶

◀

▶

Back

Close

Full Screen / Esc

Printer-friendly Version

Interactive Discussion



retrieved

$$\mathbf{K} = \left. \frac{\partial F}{\partial \mathbf{x}} \right|_{\hat{\mathbf{x}}_i, b} \quad (5)$$

In most situations commonly encountered in microwave remote sensing of the atmosphere \mathbf{x} mainly contains the profiles of different atmospheric species or of the temperature (e.g. Palm et al., 2010; Staehli et al., 2013; Tschanz et al., 2013). In this case the rows of the Jacobian look similar to the ones in WIRA's ozone retrieval shown in Fig. 4. They are positive and symmetric around the centre frequency of the emission line, meaning that a higher ozone concentration leads to higher measured brightness temperatures at all frequencies. Because of pressure broadening the higher altitudes (low pressure) mainly contribute to the signal in the central channels whereas lower altitudes (high pressure) also contribute to the signal on the wings of the measured spectrum.

In the situation of wind retrievals the functions in the rows of \mathbf{K} are of a different type (Fig. 5). The effect of the line of sight wind profile can be thought of as applying a frequency shift to the absorption coefficients of the contributing molecules at each altitude. Therefore, in contrast to species or temperature profile retrievals where the effect on the measured spectra is basically a shift in intensity space the effect of wind can be understood as a shift of parts of the spectra in frequency space. This manifests itself in the point symmetric behaviour of the rows of the Jacobian around the point (centre frequency, 0) being all negative on the one side of the centre frequency and all positive on the other side. In practice a major advantage of this behaviour is that calibration errors, which in our narrow band measurement situation can be assumed to cause a frequency independent offset or stretching of the spectrum in the intensity dimension, do not directly influence the wind retrieval. Due to pressure broadening the functions in the rows of \mathbf{K} corresponding to altitudes below 30 km are nearly frequency independent over the range covered by our spectrometer and their amplitude is very small. This illustrates the lower limit of the altitude range that WIRA is sensitive to. On

**Ground-based
middle-atmospheric
wind radiometry**

R. Rüfenacht et al.

Title Page

Abstract

Introduction

Conclusions

References

Tables

Figures



Back

Close

Full Screen / Esc

Printer-friendly Version

Interactive Discussion



the other hand the small amplitudes above 85 km indicate that not much information about these altitudes is contained in the measurements from WIRA.

Figures 4 and 5 also give an indication of the strengths of the effect of ozone variations and wind on the measured spectra. For the ozone retrieval the values of \mathbf{K} normalised by the layer thickness of the retrieval grid are typically in the order of $0.1 \text{ K ppm}^{-1} \text{ km}^{-1}$. With ozone variations in the atmosphere being in the order of 1 ppm they influence the measured spectra in the order of 0.1 K km^{-1} . For wind the normalised values of the Jacobian lie typically around $0.03 \text{ mK (m s}^{-1})^{-1} \text{ km}^{-1}$ and the atmospheric variations are in the order of 100 m s^{-1} , i.e. the influence on the measured spectra is of the order of 3 mK km^{-1} . Therefore we can state that the effect of wind variations on the measured brightness temperature spectra is approximately thirty times smaller than for species profile retrievals.

In order to conclude from the measured brightness spectra to the state of the atmosphere (wind profile, ozone profile, etc.) the inverse problem has to be solved, i.e. Eq. (4) has to be inverted. However, this is an ill-posed problem so that statistical a priori constraints need to be imposed in order to obtain a realistic solution. The “optimal” solution in the sense of Rodgers (2000) minimises the cost function

$$\chi^2 = (\mathbf{x} - \mathbf{x}_a)^T \mathbf{S}_a^{-1} (\mathbf{x} - \mathbf{x}_a) + (\mathbf{y} - F(\mathbf{x}, \mathbf{b}))^T \mathbf{S}_e^{-1} (\mathbf{y} - F(\mathbf{x}, \mathbf{b})) \quad (6)$$

where \mathbf{x}_a contains prior knowledge about the behaviour of the atmosphere (in form of realistic species or wind profiles) along with some statistics mapped into the covariance matrix \mathbf{S}_a which defines the strengths of the constraint and the correlation between different parameters/altitude levels. The wind retrieval is of non-linear type so that the solution has to be found iteratively. Applying the Levenberg-Marquardt iteration scheme (Marquardt, 1963; Press et al., 2007) the iteration step to be taken reads as

$$\hat{\mathbf{x}}_{i+1} = \hat{\mathbf{x}}_i + \left((1 + \gamma) \mathbf{S}_a^{-1} + \mathbf{K}_i^T \mathbf{S}_e^{-1} \mathbf{K}_i \right)^{-1} \left(\mathbf{K}_i^T \mathbf{S}_e^{-1} (\mathbf{y} - F(\hat{\mathbf{x}}_i, \mathbf{b})) - \mathbf{S}_a^{-1} (\hat{\mathbf{x}}_i - \mathbf{x}_a) \right) \quad (7)$$

with $\hat{\mathbf{x}}_i$ being the retrieved solution after the i th iteration step. The damping factor γ is varied according to Press et al. (2007).

Ground-based middle-atmospheric wind radiometry

R. Rüfenacht et al.

Title Page

Abstract

Introduction

Conclusions

References

Tables

Figures



Back

Close

Full Screen / Esc

Printer-friendly Version

Interactive Discussion



4 WIRA's retrieval setup

An extension of the radiative transfer simulation and inversion software package ARTS/QPACK (Eriksson et al., 2011, 2005) made it usable for wind retrievals from WIRA data. To allow this, ARTS now includes an input variable for the wind field, which is used to calculate Doppler shifts in the radiative transfer calculations, which are then handed down to the absorption calculation.

ARTS has two different ways to deal with the absorption calculation, “lookup”, or “on the fly”, which are discussed in Buehler et al. (2011). In the first case, absorption is precalculated and stored in a lookup table. When Doppler shift is present, absorption is needed for slightly different frequencies than the precalculated ones, and thus has to be interpolated. This approach is similar to the approach used in the initial simple wind retrievals by Rüfenacht et al. (2012). It can however pose numerical difficulties, since the dependence of the measured spectra on the Doppler shift is quite nonlinear.

In the second case, “on the fly” absorption, the Doppler shift calculation is exact, since absorption is calculated completely from scratch (line by line) inside the radiative transfer calculation, and this calculation is simply done for slightly shifted frequencies compared to the zero wind case. It is this option that was used for the new retrievals presented here. For both absorption cases, wind Jacobians are calculated by ARTS semi-analytically, i.e. the difference in absorption due to wind is propagated analytically through the radiative transfer, following the mathematical chain rule for derivatives. The general approach is described in Buehler et al. (2005).

WIRA's retrieval is a combined retrieval which simultaneously determines wind, ozone, (continuum) water vapour and a second order polynomial for basic corrections of baseline issues. In our measurement scheme the water vapour can basically be regarded as a correction term for tropospheric absorption and emission. To a large extent also calibration errors go into this term. Calibration inaccuracies are due to the assumption of a homogeneous troposphere in the tipping curve gain calibration process in cases where this is not exactly true (see Rüfenacht et al., 2012;

AMTD

7, 7717–7752, 2014

Ground-based middle-atmospheric wind radiometry

R. Rüfenacht et al.

Title Page

Abstract

Introduction

Conclusions

References

Tables

Figures



Back

Close

Full Screen / Esc

Printer-friendly Version

Interactive Discussion



Ground-based middle-atmospheric wind radiometry

R. Rüfenacht et al.

Title Page

Abstract

Introduction

Conclusions

References

Tables

Figures

◀

▶

◀

▶

Back

Close

Full Screen / Esc

Printer-friendly Version

Interactive Discussion



where $\sigma_{u,v}$ is the temporal standard deviation of daily average zonal or meridional profiles from ECMWF depending on location. The values for σ_u typically lie around 20 m s^{-1} at 10 hPa and 40 m s^{-1} at 1 hPa whereas σ_v takes values in the order of 10 m s^{-1} at 10 hPa and 16 m s^{-1} at 1 hPa, except at tropical latitudes where they are smaller. The correlation length for the construction of the full covariance matrix has been chosen to be 0.5 pressure decades, i.e. 8 km. For ozone and water vapour seasonally varying a priori profiles have been used. This retrieval setup is able to suppress oscillations and guarantees realistic output profiles while the influence of the a priori profile is kept minimal as shown in Fig. 7. Wind profiles retrieved with a priori profiles differing by 100 m s^{-1} vary by not more than 8 m s^{-1} in the region with high measurement response. Therefore we can state that retrieval results are not significantly biased even in situations where the zero wind a priori assumption is far from the real state of the atmosphere.

4.2 Altitude information and retrieval diagnostics

In optimal estimation techniques the averaging kernel matrix \mathbf{A} characterises the response of the retrieved profile $\hat{\mathbf{x}}$ to the “true” profile \mathbf{x} , i.e. $\mathbf{A} = \partial \hat{\mathbf{x}} / \partial \mathbf{x}$. The rows of \mathbf{A} , which are also referred to as averaging kernels, thus describe the sensitivity of a certain altitude level to perturbations from other levels. It can be shown that

$$\hat{\mathbf{x}} = \mathbf{x}_a + \mathbf{A}(\mathbf{x} - \mathbf{x}_a). \quad (9)$$

Thus the sum of the rows of \mathbf{A} , called measurement response, indicates to which extent the actual measurement contributes to the retrieval solution and how large the influence of the a priori is at the respective altitude. The averaging kernels and the measurement response of WIRA’s wind retrieval are plotted in Fig. 8. The values for the single sideband receiver shown in Fig. 8a are based on data measured with half of the integration time on the sky compared to Fig. 8b because not only zonal but also the meridional wind was measured at this time.

The difference between the peak altitude of the averaging kernels and the nominal altitude of the respective level gives an indication of the altitude accuracy of the retrieval. As an estimator for the altitude resolution the full width at half maximum of the averaging kernels can be used.

In the post processing of the wind retrieval data three conditions have been used to define the trustable altitude range of the wind data from WIRA: the measurement response must be higher than 0.8, the altitude resolution smaller than one pressure decade (16 km), and the altitude accuracy better than one quarter of a pressure decade (4 km). Data outside this range are disregarded. Figure 9 gives an overview of the altitude dependence of these quantities in typical measurement situations.

When comparing the single and double sideband receiver mode in Figs. 8 and 9 it appears that the averaging kernels for the single sideband receiver are slightly sharper, that its trustable altitude region is a little larger and that the altitude resolution and that the altitude resolution has improved by 1.5 km on average. The biggest difference between the single and double sideband mode, however, appears in the wind estimation error described in the next section.

4.3 Error analysis

The optimal estimation technique as described by Rodgers (2000) offers the diagnostic quantities of the smoothing and observation error to give estimates of the uncertainty of the retrieved profile. As mentioned before the influence of calibration inaccuracies can be neglected for the wind retrieval due to the antisymmetric behaviour of the rows of the Jacobian and the effect of fluctuations of the reference frequency is marginal.

The estimates for the smoothing and observation errors provided by the optimal estimation method might be biased by the choice of the a priori covariance. However, the smoothing error basically delivers the same information as the averaging kernels **A** shown in Fig. 8 and can thus be omitted as long as in intercomparisons the profiles to which WIRA is compared to are convolved with **A**. The observation error describes the

Ground-based middle-atmospheric wind radiometry

R. Rüfenacht et al.

Title Page

Abstract

Introduction

Conclusions

References

Tables

Figures



Back

Close

Full Screen / Esc

Printer-friendly Version

Interactive Discussion



fluctuation of the resulting profiles due to measurement noise. Therefore a more direct and robust way to estimate it is by means of Monte Carlo simulations.

For four sample days synthetic spectra have been calculated by radiative transfer modelling of the atmosphere from sample profiles of wind, ozone and water vapour.

Noise corresponding to different typical noise levels of WIRA measurements has been added to these spectra before they were fed into the retrieval algorithm to test its ability to reproduce the “true” state of the atmosphere. Results are shown in Figs. 10 and 11. Within the trustable altitude range the wind profile is well represented on average without notable bias. The standard deviation of the single retrievals plotted in Fig. 11 is an estimator for the uncertainty in the wind retrieval. It is dependent on the noise level of the input spectrum and on the receiver type (single or double sideband). Under normal measurement conditions with zenith opacities below approximately 0.3 (this corresponds to a sky containing no thick liquid water clouds) the error ranges from 17 to 27 m s^{-1} for the old double sideband receiver and from 10 to 20 m s^{-1} for the new single sideband receiver.

5 Measurements from different locations

A prototype of WIRA has been operational since September 2010. Although major upgrades as described in Sect. 2 have significantly improved the quality of the data, the measurements of the first phase before autumn 2012 (double sideband receiver) remain perfectly usable. The most notable difference is that more integration time was needed to acquire these data, thus meridional wind was not measured. Moreover the sensitive altitude range is smaller, the altitude resolution is slightly lower and the wind uncertainties are higher.

Before the upgrade to the single sideband receiver the instrument has been operated at mid latitudes (Bern, $46^{\circ}57' \text{ N}$, $7^{\circ}26' \text{ E}$) and high latitudes (Sodankylä, $67^{\circ}22' \text{ N}$, $26^{\circ}38' \text{ E}$) during 11 and 10 months respectively. After this upgrade another set of 5.5 months mid-latitudes data has been collected (Observatoire de Haute-Provence,

Ground-based middle-atmospheric wind radiometry

R. Rüfenacht et al.

Title Page

Abstract

Introduction

Conclusions

References

Tables

Figures



Back

Close

Full Screen / Esc

Printer-friendly Version

Interactive Discussion



43°56' N, 5°43' E) during a measurement campaign in the framework of the ARISE project¹. In autumn 2013 WIRA was moved to Observatoire du Maïdo on La Réunion island (21°04' S, 55°23' E) where measurements of tropical middle-atmospheric wind have successfully been performed.

5.1 Dynamical features in the data sets from the arctic to the tropics as observed by WIRA

The time series of daily averaged wind measurements from WIRA from all measurement campaigns in comparison with the operational analysis data from ECMWF (European Center for Medium-Range Weather Forecasts) are summarised in Figs. 12 and 13. The grey lines delimit the trustable altitude range of the retrieved data as defined in Sect. 4.2. Data above and below these limits shall not be considered. The three major data gaps in the time series from La Réunion were due to a loose connector (twice) and an interruption of the measurement activity during the overpass of the strong tropical cyclone Bejisa.

The seasonal pattern of the zonal wind with the slow wind reversal around equinox is visible in the data from every mid and high latitude measurement site (Fig. 12a–c). Despite the low amount of data collected on La Réunion until now, the signature of the semi-annual oscillation is clearly visible in the mesosphere (Fig. 12d).

Interesting changes in the short time dynamical structures have also been observed by WIRA. Some examples will be pointed out in the following lines. For instance an overpass of the edge of the polar vortex over central Europe during the vortex displacement event in January 2011 caused a reversal of the zonal wind over Bern (rectangle 1 in Fig. 12a). The recovery towards the westward circulation which dominates in winter first occurred in the mesosphere before it also started in the stratosphere (rectangle 2 in Fig. 12a). A few days later in mid February 2011 another reversal of the mean flow

¹ARISE is a european project for the development of research infrastructure for atmospheric dynamics and extreme events. For more information: <http://arise-project.eu>.

Ground-based middle-atmospheric wind radiometry

R. Rüfenacht et al.

Title Page

Abstract

Introduction

Conclusions

References

Tables

Figures



Back

Close

Full Screen / Esc

Printer-friendly Version

Interactive Discussion



was observed during the sudden stratospheric minor warming (rectangle 3 in Fig. 12a). Interestingly this wind reversal was confined to the stratosphere and the very low parts of the mesosphere. In the higher parts of the mesosphere the mean flow was strongly decelerated to reach nearly zero zonal wind speeds, but there was no reversal of the zonal wind direction throughout the entire middle atmosphere as it had been observed at the overpass event of mid January 2011.

At the high latitude station of Sodankylä a speedup of the westward circulation in the recovery after the major sudden stratospheric warming of January 2012 is clearly visible in the data measured by WIRA (rectangle 4 in Fig. 12b). Having a closer look at the extension and shape of the polar vortex in model data reveals that the two episodes of high zonal wind speeds in rectangle 4 coincide with periods where the edge of the vortex was unusually close to Sodankylä.

At the mid latitude station of Haute-Provence direct observations of the dynamics were made during the sudden stratospheric warming event of January 2013 (rectangle 5 in Fig. 12c). They show that the speed of the zonal wind reversed to westward direction was much higher in the mesosphere compared to the stratosphere. This is a clear contrast to the warming event of February 2011 observed at the other mid latitude station (Bern) described above where the wind reversal was confined to the lower parts of the middle atmosphere. When comparing the measurements during the January 2013 event to ECMWF model data it appears that in this special dynamical situation the zonal wind velocities measured by WIRA were slightly higher. This difference is even more notable as the ECMWF zonal wind velocities in the mesosphere are generally lower than the ones measured by WIRA (see Sect. 5.2). The January 2013 event was also the first sudden stratospheric warming during which both, the zonal and the meridional wind component, have been continuously measured thus providing complete picture of the horizontal wind field. These observations show how the mean flow at mid latitudes inverted its direction from eastward to westward by turning through the meridional direction during the SSW which resulted in unusually high meridional daily average wind

Ground-based middle-atmospheric wind radiometry

R. Rüfenacht et al.

Title Page

Abstract

Introduction

Conclusions

References

Tables

Figures



Back

Close

Full Screen / Esc

Printer-friendly Version

Interactive Discussion



velocities of beyond 50 m s^{-1} (rectangle 5 in Figs. 12c and 13a). Fair agreement in the timing of the meridional wind reversals exists between WIRA and ECMWF.

5.2 Average wind profiles of WIRA compared to ECMWF and TIDI

As already visible in Figs. 12 and 13 the agreement between the wind measured by WIRA and the ECMWF operational analysis data is good, especially in the stratosphere. However, the mesospheric zonal wind speed measured by WIRA is lower than the model wind speed from ECMWF above approximately 0.3 hPa which becomes more obvious when plotting monthly mean profiles of WIRA and ECMWF data as shown in Figs. 14 and 15. In these plots the dashed lines represent the error estimates for the averaged measurement data. In Fig. 14 data with resolutions of up to 20 km have been considered, because for the measurements made with the old double sideband receiver the altitude range where the resolution is better than 16 km can be quite limited over long time periods, especially for the Sodankylä campaign. The discrepancy in mesospheric zonal wind from WIRA and the ECMWF data convolved with WIRA's averaging kernels can be as high as 40 % in the mesosphere. Figure 16 shows the relative difference to the convolved ECMWF data for the mean profiles over the entire campaigns of Bern (1 September 2010 to 31 July 2011), Sodankylä (1 October 2011 to 31 July 2012) and Haute-Provence (20 November 2012 to 6 May 2013). The results from La Réunion are not plotted because the average zonal wind profile is very close to zero so that the relative differences do not deliver any meaningful information. All three difference profiles follow a similar pattern with agreement within 10 % in the stratosphere and significantly higher ECMWF wind speeds above 0.3 hPa.

The mesospheric zonal wind discrepancy between WIRA and ECMWF also appears when comparing convolved data. It can thus not be attributed to an artefact of WIRA averaging in smaller wind velocities from the higher parts of the mesosphere due to the limited altitude resolution. The authors do not see any reason why WIRA's zonal wind measurements should suffer from a systematical error in the mesosphere but not

Ground-based middle-atmospheric wind radiometry

R. Rüfenacht et al.

Title Page

Abstract

Introduction

Conclusions

References

Tables

Figures



Back

Close

Full Screen / Esc

Printer-friendly Version

Interactive Discussion



measurement of the meridional wind to obtain a full picture of the horizontal wind field of the atmosphere.

With measurements at four different sites between 67° N and 21° S including direct observations of sudden stratospheric warmings and displacement events of the polar vortex the data set collected by WIRA offers a great number of opportunities for further atmospheric research.

The comparison to ECMWF model data reveals good agreement in the daily average meridional wind. The zonal winds below approximately 0.3 hPa are also in good agreement. A notable difference is that ECMWF wind speeds in the mesosphere, where the model gets virtually no input data, are by up to 40 % higher than the ones measured by WIRA.

Acknowledgements. This work has been supported by the Swiss National Science Foundation grant number 200020-146388. We acknowledge ECMWF for the operational analysis data as well as NASA and University of Michigan for the TIDI wind data. We especially thank the staff of the Observatoire du Maïdo, of the Observatoire de Haute-Provence and of the Finnish Meteorological Institute in Sodankylä for the hospitality and support during the measurement campaigns.

References

Angot, G., Keckhut, P., Hauchecorne, A., and Claud, C.: Contribution of stratospheric warmings to temperature trends in the middle atmosphere from the lidar series obtained at Haute-Provence Observatory (44 degrees N), *J. Geophys. Res.-Atmos.*, 117, D21102, doi:10.1029/2012JD017631, 2012. 7726

Baldwin, M. and Dunkerton, T.: Stratospheric harbingers of anomalous weather regimes, *Science*, 294, 581–584, doi:10.1126/science.1063315, 2001. 7718

Baumgarten, G.: Doppler Rayleigh/Mie/Raman lidar for wind and temperature measurements in the middle atmosphere up to 80 km, *Atmos. Meas. Tech.*, 3, 1509–1518, doi:10.5194/amt-3-1509-2010, 2010. 7718

Ground-based middle-atmospheric wind radiometry

R. Rüfenacht et al.

Title Page

Abstract

Introduction

Conclusions

References

Tables

Figures



Back

Close

Full Screen / Esc

Printer-friendly Version

Interactive Discussion



**Ground-based
middle-atmospheric
wind radiometry**

R. Rüfenacht et al.

Title Page

Abstract

Introduction

Conclusions

References

Tables

Figures



Back

Close

Full Screen / Esc

Printer-friendly Version

Interactive Discussion



- Buehler, S. A., Eriksson, P., Kuhn, T., von Engel, A., and Verdes, C.: ARTS, the atmospheric radiative transfer simulator, *J. Quant. Spectrosc. Ra.*, 91, 65–93, doi:10.1016/j.jqsrt.2004.05.051, 2005. 7725
- Buehler, S. A., Eriksson, P., and Lemke, O.: Absorption lookup tables in the radiative transfer model ARTS, *J. Quant. Spectrosc. Ra.*, 112, 1559–1567, doi:10.1016/j.jqsrt.2011.03.008, 2011. 7725
- Burrows, S. M.: High-latitude remote sensing of mesospheric wind speeds and carbon monoxide, *J. Geophys. Res.-Atmos.*, 112, D17109, doi:10.1029/2006JD007993, 2007. 7719
- Chu, Y. H., Su, C. L., Larsen, M. F., and Chao, C. K.: First measurements of neutral wind and turbulence in the mesosphere and lower thermosphere over Taiwan with a chemical release experiment, *J. Geophys. Res.-Space*, 112, A02301, doi:10.1029/2005JA011560, 2007. 7718
- Eriksson, P., Jimenez, C., and Buehler, S.: Qpack, a general tool for instrument simulation and retrieval work, *J. Quant. Spectrosc. Ra.*, 91, 47–64, doi:10.1016/j.jqsrt.2004.05.050, 2005. 7725
- Eriksson, P., Buehler, S., Davis, C., Emde, C., and Lemke, O.: ARTS, the atmospheric radiative transfer simulator, version 2, *J. Quant. Spectrosc. Ra.*, 112, 1551–1558, doi:10.1016/j.jqsrt.2011.03.001, 2011. 7725
- Goldberg, R. A., Fritts, D. C., Williams, B. P., Lübken, F.-J., Rapp, M., Singer, W., Latteck, R., Hoffmann, P., Mullemann, A., Baumgarten, G., Schmidlin, F.-J., She, C., and Krueger, D. A.: The MaCWAVE/MIDAS rocket and ground-based measurements of polar summer dynamics: overview and mean state structure, *Geophys. Res. Lett.*, 31, L24S02, doi:10.1029/2004GL019411, 2004. 7718
- Hardiman, S. C., Butchart, N., Charlton-Perez, A. J., Shaw, T. A., Akiyoshi, H., Baumgaertner, A., Bekki, S., Braesicke, P., Chipperfield, M., Dameris, M., Garcia, R. R., Michou, M., Pawson, S., Rozanov, E., and Shibata, K.: Improved predictability of the troposphere using stratospheric final warmings, *J. Geophys. Res.-Atmos.*, 116, D18113, doi:10.1029/2011JD015914, 2011. 7718
- Killeen, T. L., Wu, Q., Solomon, S. C., Ortland, D. A., Skinner, W. R., Niciejewski, R. J., and Gell, D. A.: TIMED Doppler interferometer: overview and recent results, *J. Geophys. Res.-Space*, 111, A10S01, doi:10.1029/2005JA011484, 2006. 7733
- Marquardt, D.: An algorithm for least-squares estimation of nonlinear parameters, *J. Soc. Ind. Appl. Math.*, 11, 431–441, doi:10.1137/0111030, 1963. 7724

Ground-based middle-atmospheric wind radiometry

R. Rüfenacht et al.

Title Page

Abstract

Introduction

Conclusions

References

Tables

Figures



Back

Close

Full Screen / Esc

Printer-friendly Version

Interactive Discussion



Palm, M., Hoffmann, C. G., Golchert, S. H. W., and Notholt, J.: The ground-based MW radiometer OZORAM on Spitsbergen – description and status of stratospheric and mesospheric O₃-measurements, *Atmos. Meas. Tech.*, 3, 1533–1545, doi:10.5194/amt-3-1533-2010, 2010. 7723

5 Press, W. H., Teukolsky, S. A., Vetterling, W. T., and Flannery, B. P.: Numerical Recipes 3rd Edition: The Art of Scientific Computing, 3rd edn., Cambridge University Press, New York, NY, USA, 2007. 7724

Rodgers, C. D.: Inverse methods for atmospheric sounding: theory and practice, in: Series on Atmospheric, Oceanic and Planetary Physics, vol. 2, World Scientific, Singapore, reprint 2008, 2000. 7721, 7724, 7728

10 Rüfenacht, R., Kämpfer, N., and Murk, A.: First middle-atmospheric zonal wind profile measurements with a new ground-based microwave Doppler-spectro-radiometer, *Atmos. Meas. Tech.*, 5, 2647–2659, doi:10.5194/amt-5-2647-2012, 2012. 7719, 7720, 7721, 7725

Schneebeli, M. and Mätzler, C.: A calibration scheme for microwave radiometers using tipping curves and kalman filtering, *IEEE T. Geosci. Remote*, 47, 4201–4209, doi:10.1109/TGRS.2009.2023784, 2009. 7726

15 Stähli, O., Murk, A., Kämpfer, N., Mätzler, C., and Eriksson, P.: Microwave radiometer to retrieve temperature profiles from the surface to the stratopause, *Atmos. Meas. Tech.*, 6, 2477–2494, doi:10.5194/amt-6-2477-2013, 2013. 7723

20 Tschanz, B., Straub, C., Scheiben, D., Walker, K. A., Stiller, G. P., and Kämpfer, N.: Validation of middle-atmospheric campaign-based water vapour measured by the ground-based microwave radiometer MIAWARA-C, *Atmos. Meas. Tech.*, 6, 1725–1745, doi:10.5194/amt-6-1725-2013, 2013. 7723

25 Verdes, C., Buehler, S., Perrin, A., Flaud, J., Demaison, J., Wlodarczak, G., Colmont, J., Cazzoli, G., and Puzzarini, C.: A sensitivity study on spectroscopic parameter accuracies for a mm/sub-mm limb sounder instrument, *J. Mol. Spectrosc.*, 229, 266–275, doi:10.1016/j.jms.2004.09.014, 2005. 7722



Figure 1. WIRA's frontend during its operation at the Observatoire du Maïdo on La Réunion island.

AMTD

7, 7717–7752, 2014

Ground-based middle-atmospheric wind radiometry

R. Rüfenacht et al.

Title Page

Abstract

Introduction

Conclusions

References

Tables

Figures

◀

▶

◀

▶

Back

Close

Full Screen / Esc

Printer-friendly Version

Interactive Discussion



Ground-based middle-atmospheric wind radiometry

R. Rüfenacht et al.

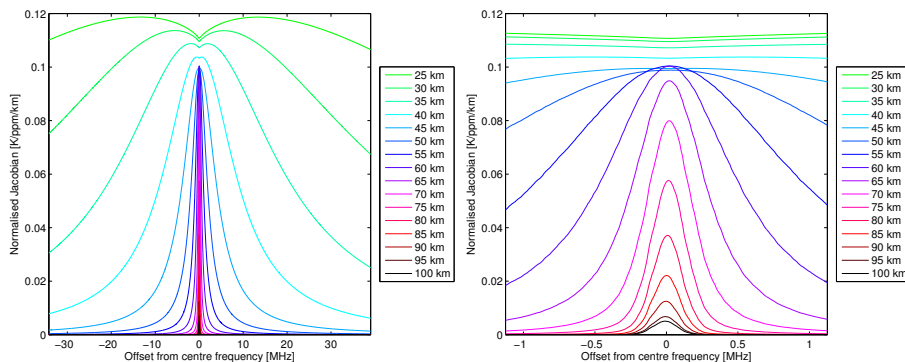


Figure 4. Rows of the Jacobian describing WIRA's ozone retrieval normalised by the layer thickness of the retrieval grid for observations at 22° elevation. Full usable spectrometer bandwidth (left) and zoom on the central channels (right).

Title Page

Abstract

Introduction

Conclusions

References

Tables

Figures

◀

▶

◀

▶

Back

Close

Full Screen / Esc

Printer-friendly Version

Interactive Discussion



Ground-based middle-atmospheric wind radiometry

R. Rüfenacht et al.

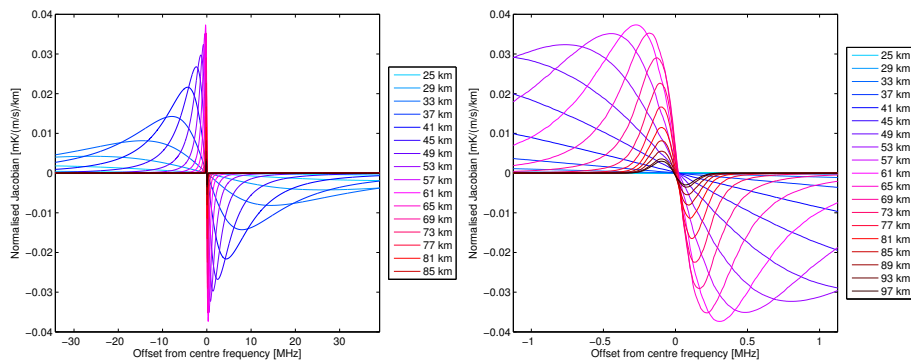


Figure 5. Rows of the Jacobian describing WIRA's horizontal wind retrieval normalised by the layer thickness of the retrieval grid for observations at 22° elevation. Full usable spectrometer bandwidth (left) and zoom on the central channels (right).

Title Page

Abstract

Introduction

Conclusions

References

Tables

Figures

◀

▶

◀

▶

Back

Close

Full Screen / Esc

Printer-friendly Version

Interactive Discussion



**Ground-based
middle-atmospheric
wind radiometry**

R. Rüfenacht et al.

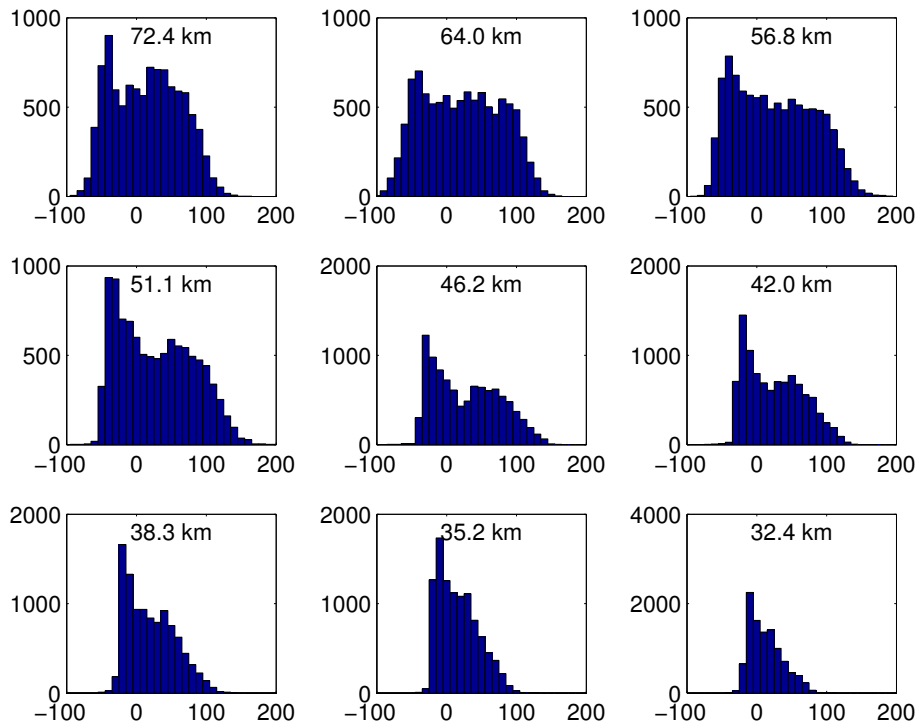


Figure 6. Distribution of zonal wind speeds on different altitude levels according to ECMWF operational analysis data. In this example six years of data for Bern have been used.

[Title Page](#)[Abstract](#)[Introduction](#)[Conclusions](#)[References](#)[Tables](#)[Figures](#)[◀](#)[▶](#)[◀](#)[▶](#)[Back](#)[Close](#)[Full Screen / Esc](#)[Printer-friendly Version](#)[Interactive Discussion](#)

Ground-based middle-atmospheric wind radiometry

R. Rüfenacht et al.

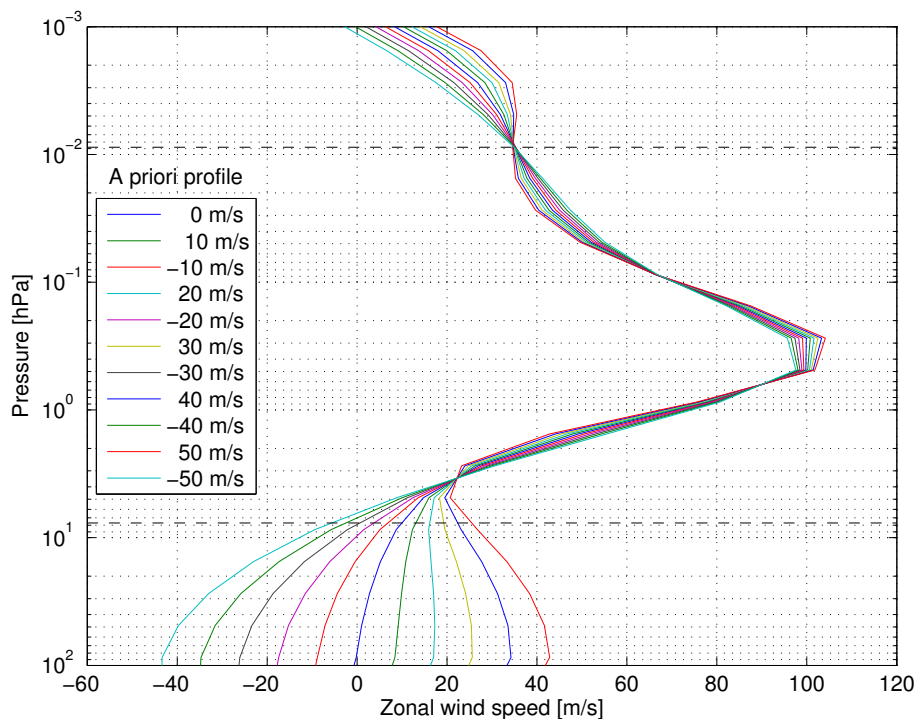


Figure 7. Influence of different choices of constant a priori wind profiles (indicated in the legend box) on the retrieval result for a real measurement example (23 November 2013). The dashed horizontal lines represent the limits where the measurement response is higher than 0.8. Within this altitude range the influence of the choice of the a priori profile is small.

Title Page

Abstract

Introduction

Conclusions

References

Tables

Figures

◀

▶

◀

▶

Back

Close

Full Screen / Esc

Printer-friendly Version

Interactive Discussion



Ground-based middle-atmospheric wind radiometry

R. Rüfenacht et al.

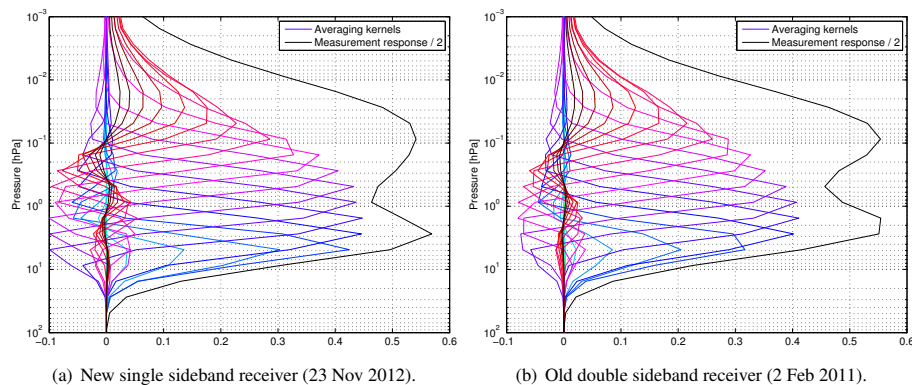


Figure 8. Typical sets of WIRA wind averaging kernels and measurement response.

Title Page

Abstract

Introduction

Conclusions

References

Tables

Figures



Back

Close

Full Screen / Esc

Printer-friendly Version

Interactive Discussion



Ground-based middle-atmospheric wind radiometry

R. Rüfenacht et al.

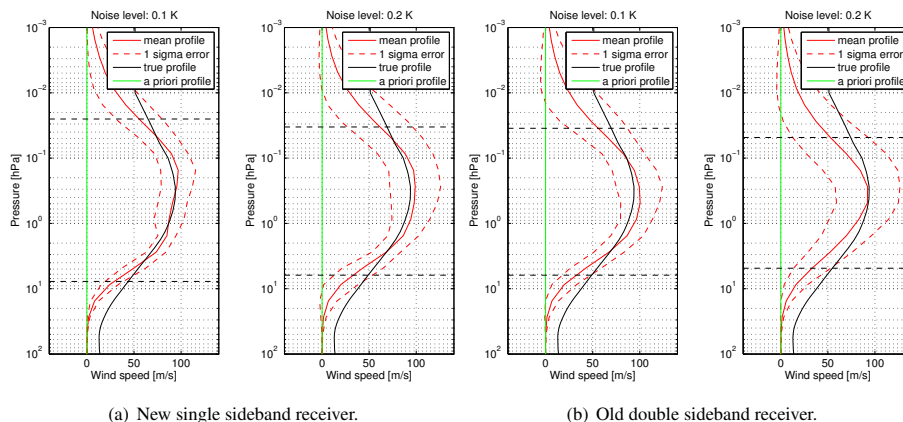


Figure 10. Monte Carlo error simulations for typical noise levels for days with clear sky or dry clouds (noise level 0.1 K) and high opacity as in the case of wet clouds (noise level 0.2 K). The horizontal lines delimit the trustable altitude region. The true profile is the wind profile that was used to generate the synthetic spectra that were fed to the retrieval algorithm.

**Ground-based
middle-atmospheric
wind radiometry**

R. Rüfenacht et al.

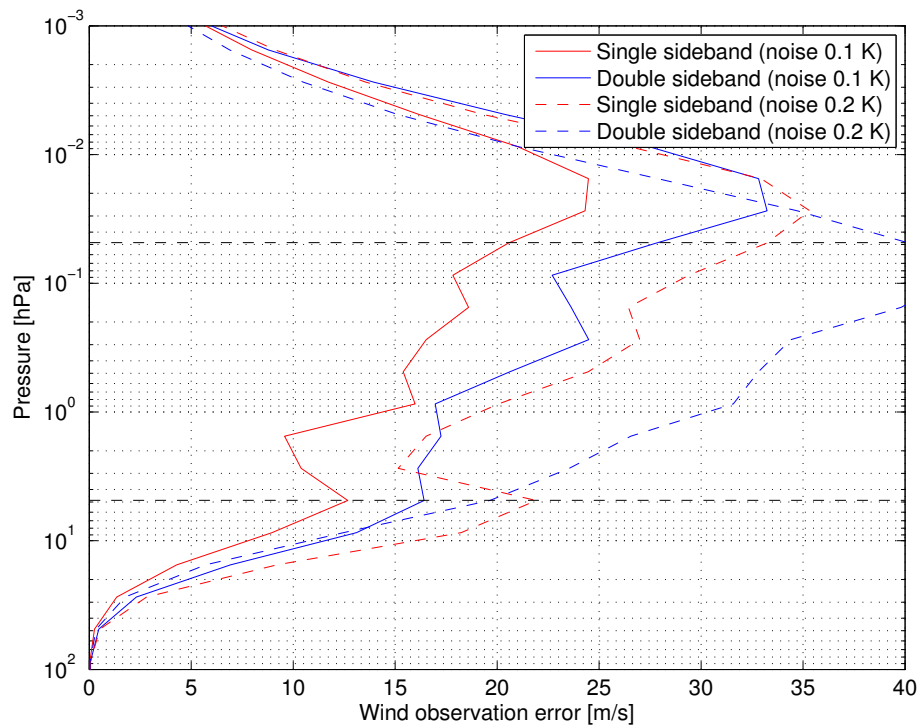


Figure 11. Standard deviation of the resulting profiles in the Monte Carlo simulation displayed in Fig. 10.

[Title Page](#)[Abstract](#)[Introduction](#)[Conclusions](#)[References](#)[Tables](#)[Figures](#)[◀](#)[▶](#)[◀](#)[▶](#)[Back](#)[Close](#)[Full Screen / Esc](#)[Printer-friendly Version](#)[Interactive Discussion](#)

Ground-based middle-atmospheric wind radiometry

R. Rüfenacht et al.

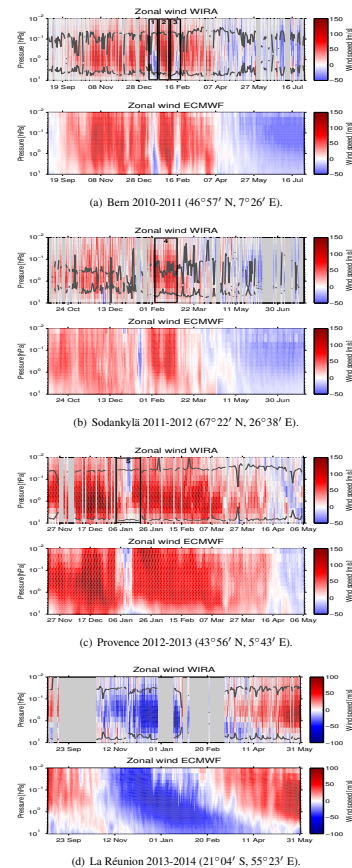


Figure 12. Zonal wind time series measured by WIRA at four different locations compared to ECMWF operational analysis data. The grey lines delimit the trustable altitude range of the retrieved data. The black rectangles mark the dynamic episodes described in the text.

Title Page

Abstract

Introduction

Conclusions

References

Tables

Figures



Back

Close

Full Screen / Esc

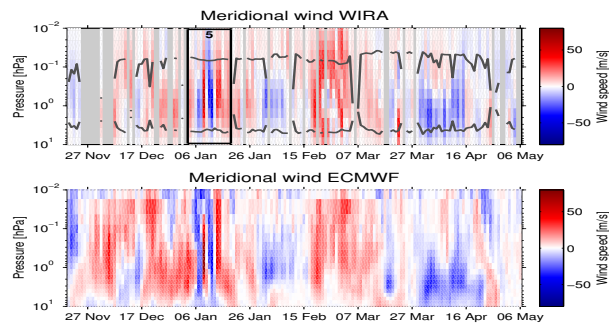
Printer-friendly Version

Interactive Discussion

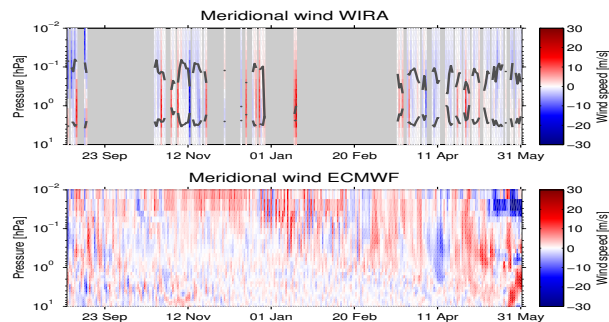


Ground-based middle-atmospheric wind radiometry

R. Rüfenacht et al.



(a) Provence 2012-2013 ($43^{\circ}56' \text{ N}$, $5^{\circ}43' \text{ E}$).



(b) La Réunion 2013-2014 ($21^{\circ}04' \text{ S}$, $55^{\circ}23' \text{ E}$).

Figure 13. Meridional wind time series measured by WIRA at two different locations compared to ECMWF operational analysis data. The grey lines delimit the trustable altitude range of the retrieved data. The black rectangle marks a dynamic episode described in the text.

Title Page

Abstract

Introduction

Conclusions

References

Tables

Figures



Back

Close

Full Screen / Esc

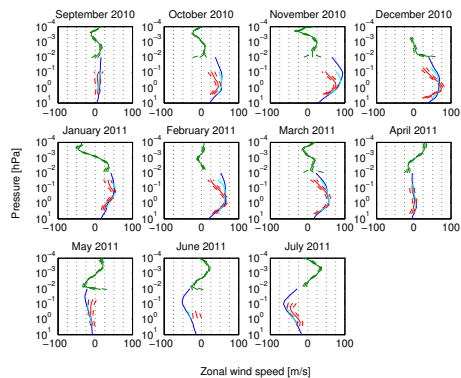
Printer-friendly Version

Interactive Discussion

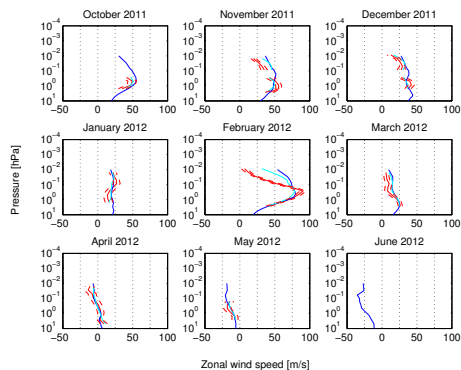


Ground-based
middle-atmospheric
wind radiometry

R. Rufenacht et al.



(a) Bern 2010–2011 (46°57' N, 7°26' E).



(b) Sodankylä 2011–2012 (67°22' N, 26°38' E).

Figure 14. Monthly mean profiles of zonal wind measured by the old WIRA double sideband receiver (red) compared to ECMWF operational analysis data (blue), to the ECMWF profile convolved with WIRA's averaging kernels (cyan) and to TIDI data (green).

Title Page

Abstract

Introduction

Conclusions

References

Tables

Figures



Back

Close

Full Screen / Esc

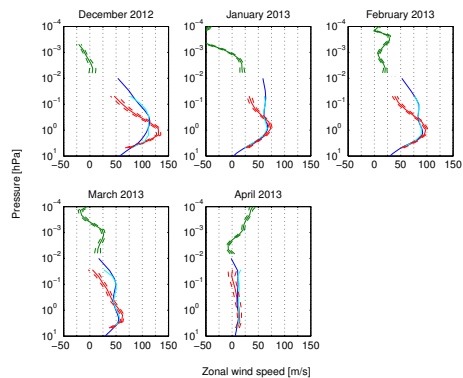
Printer-friendly Version

Interactive Discussion

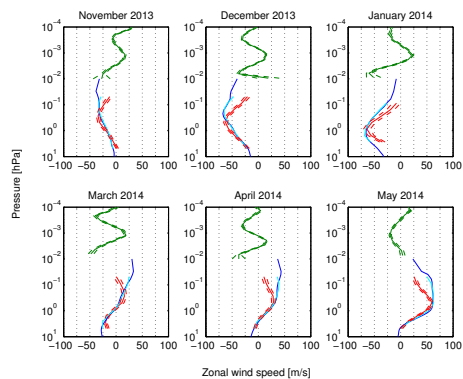


Ground-based
middle-atmospheric
wind radiometry

R. Rüfenacht et al.



(a) Provence 2012-2013 (43°56' N, 5°43' E).



(b) La Réunion 2013-2014 (21°04' S, 55°23' E).

Figure 15. Monthly mean profiles of zonal wind measured by the new WIRA single sideband receiver (red) compared to ECMWF operational analysis data (blue), to the ECMWF profile convolved with WIRA's averaging kernels (cyan) and to TIDI data (green).

Title Page

Abstract

Introduction

Conclusions

References

Tables

Figures



Back

Close

Full Screen / Esc

Printer-friendly Version

Interactive Discussion



